SCIENCE CHINA
Earth Sciences

•ARTICLE•

January 2024 Vol.67 No.1: 208–221
https://doi.org/10.1007/s11430-022-1164-2

Microbially-mediated formation of Ca-Fe carbonates during dissimilatory ferrihydrite reduction: Implications for the origin of sedimentary ankerite

Deng LIU[1,2*], Jinpeng CAO[2], Shanshan YANG[2], Yating YIN[2], Pengcong WANG[1], Dominic PAPINEAU[1,3,4,5], Hongmei WANG[1,2], Xuan QIU[1], Genming LUO[1], Zongmin ZHU[1] & Fengping WANG[6]

[1] *State Key Laboratory of Biogeology and Environmental Geology, China University of Geosciences, Wuhan 430074, China;*
[2] *School of Environmental Studies, China University of Geosciences, Wuhan 430074, China;*
[3] *London Centre for Nanotechnology, University College London, London WC1H 0AH, UK;*
[4] *Department of Earth Sciences, University College London, London WC1E 6BT, UK;*
[5] *Center for Planetary Sciences, University College London and Birkbeck College London, London WC1E 6BT, UK;*
[6] *State Key Laboratory of Microbial Metabolism, State Key Laboratory of Ocean Engineering, Shanghai Jiao Tong University, Shanghai 200240, China*

Received May 27, 2022; revised July 21, 2023; accepted August 8, 2023; published online December 14, 2023

Abstract The origin of sedimentary dolomite has become a long-standing problem in the Earth Sciences. Some carbonate minerals like ankerite have the same crystal structure as dolomite, hence their genesis may provide clues to help solving the dolomite problem. The purpose of this study was to probe whether microbial activity can be involved in the formation of ankerite. Bio-carbonation experiments associated with microbial iron reduction were performed in batch systems with various concentrations of Ca^{2+}(0–20 mmol/L), with a marine iron-reducing bacterium *Shewanella piezotolerans* WP3 as the reaction mediator, and with lactate and ferrihydrite as the respective electron donor and acceptor. Our biomineralization data showed that Ca-amendments expedited microbially-mediated ferrihydrite reduction by enhancing the adhesion between WP3 cells and ferrihydrite particles. After bioreduction, siderite occurred as the principal secondary mineral in the Ca-free systems. Instead, Ca-Fe carbonates were formed when Ca^{2+} ions were present. The $CaCO_3$ content of microbially-induced Ca-Fe carbonates was positively correlated with the initial Ca^{2+} concentration. The Ca-Fe carbonate phase produced in the 20 mmol/L Ca-amended biosystems had a chemical formula of $Ca_{0.8}Fe_{1.2}(CO_3)_2$, which is close to the theoretical composition of ankerite. This ankerite-like phase was nanometric in size and spherical, Ca-Fe disordered, and structurally defective. Our simulated diagenesis experiments further demonstrated that the resulting ankerite-like phase could be converted into ordered ankerite under hydrothermal conditions. We introduced the term "proto-ankerite" to define the Ca-Fe phases that possess near-ankerite stoichiometry but disordered cation arrangement. On the basis of the present study, we proposed herein that microbial activity is an important contributor to the genesis of sedimentary ankerite by providing the metastable Ca-Fe carbonate precursors.

Keywords Ankerite, Proto-ankerite, Microbial iron reduction, Dolomite problem, Mineral transformation

Citation: Liu D, Cao J, Yang S, Yin Y, Wang P, Papineau D, Wang H, Qiu X, Luo G, Zhu Z, Wang F. 2024. Microbially-mediated formation of Ca-Fe carbonates during dissimilatory ferrihydrite reduction: Implications for the origin of sedimentary ankerite. Science China Earth Sciences, 67(1): 208–221, https://doi.org/10.1007/s11430-022-1164-2

* Corresponding author (email: liudeng@cug.edu.cn)

1. Introduction

Crystalline calcium-bearing carbonates are important components of sediments and sedimentary rocks. These carbonate minerals have been documented as an archive of recent and past Earth's chemical and climatic changes (Higgins et al., 2018; Chang et al., 2020). Furthermore, they represent typical skeletal constituents of marine invertebrates (Marin et al., 1996), and are profoundly involved in the whole-Earth carbon cycle (Schrag et al., 2013; Liu Y et al., 2019). Despite the importance of these carbonates, their formation mechanism and kinetics are not well understood. Dolomite [$CaMg(CO_3)_2$], in particular, has been an enigmatic mineral for over two centuries. The long-lasting debate about the origin of dolomite, known as the "dolomite problem", is mainly due to the apparent mismatch between the difficulty of dolomite synthesis under ambient conditions and its widespread occurrence in sedimentary rocks (Gregg et al., 2015; Guo et al., 2017; Petrash et al., 2017).

In nature, some double carbonates such as ankerite [$CaFe(CO_3)_2$], kutnahorite [$CaMn(CO_3)_2$], and minrecordite [$CaZn(CO_3)_2$] also have the trigonal and rhombohedral structure of dolomite, and hence they are defined as dolomite group minerals (Pimentel and Pina, 2016). These double carbonates have received growing attention because insights into the formation mechanism of these minerals would provide clues to better understand the genesis of sedimentary dolomite (Liu and Li, 2020).

Ankerite is the second most common dolomite group mineral after dolomite (Gregg et al., 2015). Noticeably, "hypothetical" ankerite that has the chemical composition of $CaFe(CO_3)_2$ and Ca-Fe ordering is not found to occur naturally (Gregg et al., 2015). According to the International Mineralogical Association (IMA) guidelines, natural ankerite is a $Ca(Mg, Fe)(CO_3)_2$ carbonate, in which more than 50 mol% Mg^{2+} ions in the dolomitic structure are substituted by Fe^{2+} ions (Gregg et al., 2015; Xu et al., 2019). Similar to dolomite, ankerite does not easily precipitate from saturated solutions at Earth surface temperatures (Gregg et al., 2015; Xu et al., 2019). Therefore, sedimentary ankerite has often been proposed as a diagenetic mineral replacing calcite, for instance through the following reaction (Hendry et al., 2000):

$$4CaCO_3(\text{calcite})+Fe^{2+}+Mg^{2+}\rightarrow 2CaMg_{0.5}Fe_{0.5}(CO_3)_2(\text{ankerite})+2Ca^{2+}$$

Such replacement reaction is usually thought to require temperatures between 100°C and 200°C during deep burial (e.g., Hendry et al., 2000).

Microorganisms are cosmopolitan on Earth and they show potential to mediate the precipitation and crystallization of various minerals (Xie et al., 2016). Of particular note, considerable research, mostly based on laboratory simulation experiments, has shown that some types of microbes can overcome the magnesium-hydration barrier and catalyze the precipitation of dolomite or other Mg-Ca carbonates under low-temperature conditions (Petrash et al., 2017, and references therein). In most reports, however, microbially-induced dolomite has disordered cations and is often described as disordered proto-dolomite or very high-Mg calcite (Gregg et al., 2015). It has been suggested that low-temperature proto-dolomite can convert into their ordered counterparts during burial diagenesis and/or metamorphism (Zhang et al., 2012; Zheng et al., 2021). This emerging microbial model of dolomite formation has been applied to interpret the origin of some sedimentary dolomites (Perri and Tucker, 2007; You et al., 2014; Wen et al., 2020; Li et al., 2021). Since ankerite belongs to the dolomite group, it has been hypothesized that microorganisms might be a triggering factor for the formation of ankerite (e.g., Xu et al., 2019). Hence, laboratory experiments are needed to test this hypothesis.

In the present study, we performed cultivation experiments to test whether dissimilatory iron-reducing bacteria (DIRB) can enhance the incorporation of Ca^{2+} into Ca-Fe carbonate precipitates upon the biological reduction of ferrihydrite, which is the most common iron hydroxide found in sedimentary environments. Specifically, the Ca-Fe carbonate formed in such biological systems with a high Ca/Fe ratio tested herein had a stoichiometry close to the "theoretical" ankerite [$CaFe(CO_3)_2$], but was mostly cation disordered. We thus suggest the term of "proto-ankerite" to describe this phase since it could serve as a metastable precursor for ordered ankerite, as subsequently demonstrated in our hydrothermal experiments. Our experiments provide an alternative explanation for the origin of sedimentary ankerite, that is, low-temperature Ca-Fe carbonate precursors (e.g., proto-ankerite) are primarily stimulated by microbial activity and subsequently converted into more stable ankerite through a diagenesis-controlled recrystallization reaction.

2. Materials and methods

2.1 Bacterial strain and culture medium

The *Shewanella* strains are known for their dissimilatory Fe (III)-respiring capabilities, and they represent the most abundant *Proteobacteria* in ferruginous seafloor environments (Wang et al., 2008). *Shewanella piezotolerans* WP3, a marine facultative DIRB originally isolated from West Pacific sediments (Wang et al., 2008), was selected for this study. Cells of strain WP3 were first cultured aerobically in marine medium 2216E (with 5 g/L peptone, 1 g/L yeast extract, 0.01 g/L $FePO_4$, 34 g/L NaCl, pH=7.5) at 20°C with constant agitation (160 r/min). Once cell growth reached the mid to late log phase (as indicated by measurements of OD_{600}), WP3 cells were harvested in an anaerobic chamber

(filled with 98% N_2 and 2% H_2, Coy Laboratory Products, USA) by centrifugation (8000×g, 10 min) and resuspended in pre-deoxygenated marine salt bicarbonate buffer (2.5 g/L $NaHCO_3$, 30 g/L NaCl, 10 g/L $MgCl_2·6H_2O$, 1 g/L KCl and 1 g/L $CaCl_2$, pH=7.5). The harvested cells were kept in serum bottles in the dark at 4°C for future use.

2.2 Preparation of ferrihydrite

Ferrihydrite was prepared based on the method of Schwertmann and Cornell (1991). In brief, a 5 mol/L KOH solution was added slowly into a 1 mol/L $Fe(NO_3)_3·9H_2O$ with vigorous stirring to the pH 7–8. The mixture was allowed to stand for 3 hours at room temperature. The ferrihydrite precipitates were collected by centrifugation (8000×g, 15 min), repeatedly washed with double distilled water, and made into slurry to obtain a Fe(III) concentration of 0.3 mol/L. This slurry served as a stock solution for subsequent iron reduction experiments.

2.3 Microbial iron reduction and adhesion experiments

Batch experiments were conducted with various concentrations of Ca^{2+} to evaluate whether Ca^{2+} could be incorporated into mineral precipitates during microbial reduction of ferrihydrite. A modified basal medium for *Shewanella* species was used for microbial reduction experiments (Roden et al., 2002). The composition of the medium consisted of 30 mmol/L $NaHCO_3$, 50 mmol/L $MgCl_2$, 0.5 mmol/L KH_2PO_4, 513 mmol/L NaCl, different concentrations of $CaCl_2$ (0, 5, 10 and 20 mmol/L), 0.2 g/L yeast extract, 1 mL trace elements (Roden et al., 2002), and 1 mL vitamin solution (Roden et al., 2002). The medium pH was adjusted to 7.5 by adding 0.1 mol/L NaOH as needed. The modified basal medium was purged with ultra-pure N_2 and transferred into the anaerobic chamber for membrane filtration (MF, Millipore, USA; pore size of 0.22 μm). This filtered medium was dispensed into sterile serum bottles and sealed with butyl rubber stoppers. The serum bottles were supplemented with ferrihydrite stock solution as the sole electron acceptor (10 mmol/L, final concentration) and pre-filtered sterilized sodium lactate as the electron donor (final concentration of 20 mmol/L). An aliquot of WP3 suspension was then injected into selected bottles to achieve a final concentration of about $1×10^7$ cells/mL. In addition, abiotic controls without bacterial inoculum were also performed. Both biotic and abiotic reactors were conducted in duplicate. The experimental bottles were wrapped in aluminum foil to block light and then placed in an incubator at 20°C without agitation.

Microbial adhesion to the Fe(III) minerals is a crucial step in microbial iron reduction. To examine the influence of Ca^{2+} on microbial reduction of ferrihydrite, the adhesion experiments were performed in the aforementioned basal medium in which the organic substrates were omitted. The adhesion capacity of WP3 to ferrihydrite was determined by the methods described previously (Zhao et al., 2014). In brief, pre-washed WP3 cells were added into 30 mmol/L ferrihydrite suspensions to obtain a cell density of about $1×10^7$ cells/mL. The initial concentration of Ca^{2+} was varied in the range of 0–20 mmol/L. The cell-mineral mixtures were agitated at 150 r/min at 20°C. After a one hour-incubation period, the un-adhered cells of strain WP3 were separated from the attached cells and ferrihydrite particles by injecting 60% sucrose solution (w/w). These sucrose-amended suspensions were centrifuged at 8000×g for 10 min. The numbers of un-adhered cells in the supernatants were determined with acridine-orange direct count (AODC) by epi-fluorescence microscopy (Olympus BX50, Olympus Optical Co., Tokyo, Japan).

2.4 Hydrothermal alteration experiments

Our experiments demonstrated that strain WP3 was able to trigger the formation of Ca-Fe carbonates accompanied by the bioreduction of ferrihydrite (see later Section 3.3 for details). We hypothesized that Ca-Fe carbonate neoformations (especially proto-ankerite) could transform into ankerite during burial diagenesis. In order to test such hypothesis, hydrothermal simulation experiments were further carried out to mimic the fluid-induced mineral transformation.

Proto-ankerite that was produced in the bioreactors with 20 mmol/L Ca^{2+} was selected as a representative Ca-Fe carbonate for hydrothermal experiments. In a typical experimental run, 500 mg of proto-ankerite powder and 25 mL anaerobic marine salt bicarbonate buffer (2.5 g/L $NaHCO_3$, 30 g/L NaCl, 10 g/L $MgCl_2·6H_2O$, 1 g/L KCl and 1 g/L $CaCl_2$, pH=7.5) were loaded in a sealed Teflon-lined bomb and heated up to 100°C for two months, and then cooled to room temperature. The reaction solids were separated by centrifugation at 8000×g for 10 min. The resulting pellet was further washed with pre-deoxygenated double distilled water three times and dried in the anaerobic chamber.

2.5 Analyses

2.5.1 Wet chemistry

At each sampling point, solution pH was determined in the supernatants using a Hach multimeter (Hach Co., USA). Cell density was estimated as colony forming units (CFUs). The concentrations of NH_4^+ and solution alkalinity were determined spectrophotometrically as described by McLeod (1992) and Sarazin et al. (1999), respectively. Briefly, two mL aliquots of cell-ferrihydrite suspension were sampled at selected time points with a sterile and anoxic syringe followed by centrifugation at 8000×g for 10 min. For NH_4^+

measurement, 1 mL of the supernatant was mixed with 0.5 mL of sodium salicylate-sodium hydroxide solution and 0.2 mL of sodium dichloroisocyanurate solution. The mixture was measured with a UV-spectrophotometer (Shimadzu UV-1800, Shimadzu, Japan) at 660 nm after 30 min of reaction time. Specifically for alkalinity determination, another 1 mL of supernatant was added into an equal volume of colored reagent that consists of 0.01 mol/L formic acid and 0.05 g/L Bromophenol-Blue. Absorbances were measured at 590 nm with $NaHCO_3$ as a standard.

The concentrations of total Fe(II) and aqueous Fe(II) were analyzed by the ferrozine method (Stookey, 1970). Specifically for total Fe(II), 0.5 mL mineral slurry was withdrawn by syringe and injected into 0.5 mL of 1 mol/L HCl. After 24 h incubation in the dark, a 0.1-mL sample of the extract was added to 1 mL of ferrozine (1 g/L) in 50 mmol/L HEPES buffer. The absorbance at 562 nm was determined and compared to Fe(II) standards of ferrous ethylene diammonium sulfate. Aqueous Fe(II) concentration was measured after filtering the mineral slurry through a syringe membrane filter (0.22 μm). Samples of Ca^{2+} and Mg^{2+} ions were collected from the supernatants following centrifugation (8000×g, 15 min) and their concentrations were measured with inductively coupled plasma-optical emission spectrometry (ICP-OES, Thermofisher ICAP6300, USA).

2.5.2 Mineral characterization

The zeta potential (ξ) of ferrihydrite suspension in the uninoculated medium as a function of different concentrations of Ca^{2+} was measured using a Zeta potential analyzer (ZetaSizer Nano ZS, Malvern Instruments, UK). The bioreduced samples were characterized by X-ray diffraction (XRD), scanning electron microscopy (SEM), and transmission electron microscopy (TEM). Prior to XRD measurements, samples were washed with pre-deoxygenated water three times to remove residual salts and dried at 20°C in an anaerobic chamber. The mineral powders were X-rayed from 10° to 60° 2θ using a Bruker D8 Advance XRD (Bruker, Germany) with Cu Kα radiation at 40 kV and 40 mA. The XRD data were analyzed with JADE 6.0 software (MDI, Livermore, USA) to identify phase. The morphology and chemical composition of biogenic minerals before and after hydrothermal treatments were examined using a Hitachi SU8010 SEM (Hitachi, Japan), which is equipped with an energy dispersive X-ray spectroscopy (EDS) detector (Oxford Instruments XMax 80, UK). The samples for SEM observation were Pt-coated prior to analysis. Then, samples were prepared for TEM analysis by dispersing the mineral powders in ethanol under ultra-sonication and depositing the product on carbon-coated 300 mesh copper grids. TEM observations were performed using a JEOL JEM-2100F (JEOL, Japan) with a LaB_6 source, operating at 200 kV. The observations were carried out in the modes of bright field imaging and selected area electron diffraction (SAED). Crystallographic analysis of TEM images was performed using DigitalMicrograph software (Gatan Inc., USA). The elemental distribution of solid phases was also studied by ICP-OES after digestion with HNO_3 (trace metal grade).

3. Results

3.1 Changes in wet chemistry during microbial iron reduction

During the incubation period, the pH in the bioreactors steadily increased within the first 15 days and then leveled off with time (Figure 1a). At the end of experiments (50 days), the pH rose from an initial value of ca. 7.50 to 8.36, 8.21, 7.90 and 8.04 in the biosystems with 0, 5, 10 and 20 mmol/L Ca^{2+}, respectively. The pH in the abiotic reactors increased slightly to 7.74 after 50 days. There were no CFUs observed in the abiotic controls. In contrast, the cell density in the bioreactors exhibited a rapid rise for the first 7 or 10 days but a gradual decline afterwards (Figure 1b). Whereas insignificant NH_4^+ was produced in abiotic controls, the concentrations of NH_4^+ of the bioreduction experiments quickly increased within the first 7 days followed by a slower increase and a final plateau (around 5 mmol/L) (Figure 1c), which indicates that microbial ammonification took place in the incubation systems. Furthermore, the increase of solution alkalinity was also observed in the bioreactors (Figure 1d).

As illustrated in Figure 2a, a significant accumulation of total Fe(II) was detected when ferrihydrite was exposed to *S. piezotolerans* WP3, consistent with a previous study (Wu et al., 2011). Unlike the biotic experiments, a negligible change in the concentration of total Fe(II) in abiotic control experiments was observed. Moreover, it was noted that the presence of Ca led to higher rates of microbial iron reduction within the first 20 days. However, nearly similar reduction rates were observed among the Ca-containing biosystems, regardless of the amount of Ca used. A two-stage increasing trend was found in these biosystems: a rapid increase for the initial incubation period, followed by a moderate increase for the subsequent incubation period (Figure 2a). Although different initial bioreduction rates occurred with and without Ca^{2+} ions, the final extents of ferrihydrite reduction were comparable at 76.4%, 77.7%, 83.5% and 80.0% for the bioreactors with 0, 5, 10 and 20 mmol/L Ca^{2+}, respectively. The concentrations of aqueous Fe(II) in all biotic treatments increased in the initial incubation period (30 days for Ca-free systems and 15 or 20 days for Ca-amended reactors) (Figure 2b). Subsequent to these increases, aqueous Fe(II) was gradually removed from solutions in all biotic experiments. Aqueous Mg and Ca were also measured to assess their fate

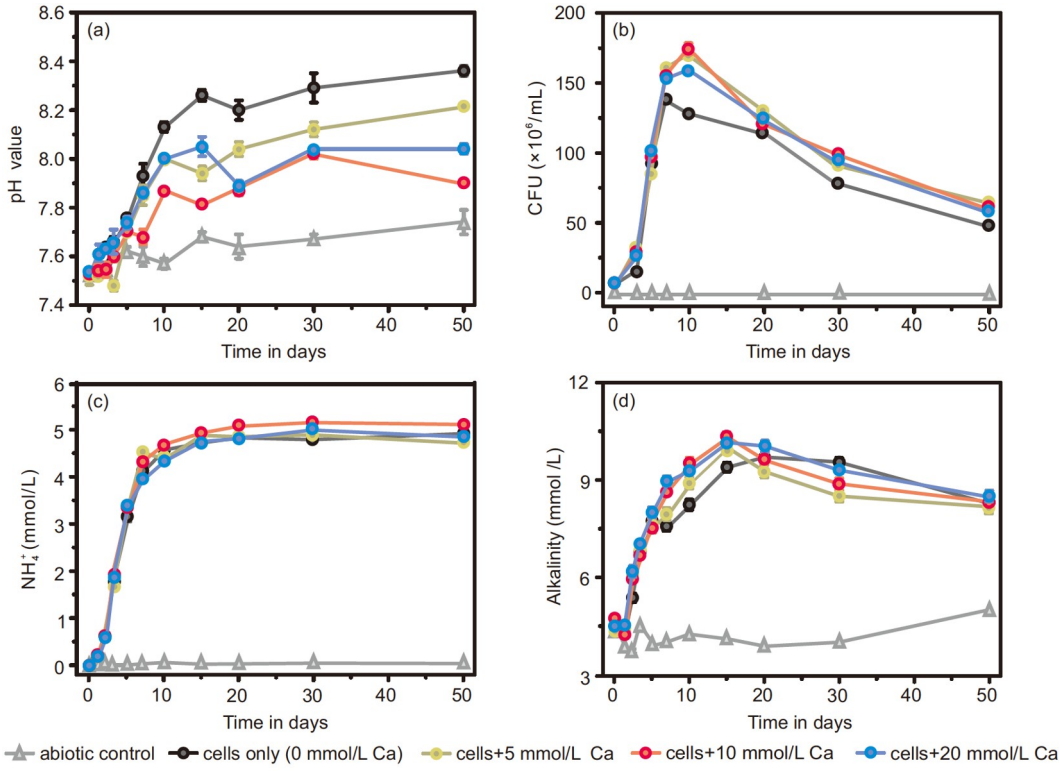

Figure 1 Time course analysis of solution during microbial reduction of ferrihydrite: (a) solution pH; (b) cell number (CFU); (c)NH_4^+; and (d) solution alkalinity. All results were from duplicate cultures.

during microbial reduction of ferrihydrite (Figure 2c and 2d). In general, during the 50-day incubation experiments, the concentrations of Mg^{2+} remained unchanged in all biological reduction experiments (Figure 2c). In contrast, a decline in Ca^{2+} ions was observed during microbial iron reduction (Figure 2d). At the end of the experiments, the removal percentages of Ca during microbial iron reduction were estimated as 31.3%, 33.0% and 23.8% for the biosystems with 5, 10, and 20 mmol/L Ca^{2+}, respectively.

3.2 Zeta potential of ferrihydrite and bacterial adhesion in the presence of Ca^{2+}

The zeta potential measurements showed that calcium ions had a significant impact on the surface electronic property of ferrihydrite particles (Figure 3). In the absence of Ca^{2+}, the ferrihydrite surface carried a slight negative charge (as indicated by the ξ values ranging from −18.2 to −13.8 mV) at pH 7–9. When Ca^{2+} ions were introduced into the mineral suspensions, the ξ values became positive and they increased with the increasing concentration of Ca^{2+} (Figure 3).

In the absence of Ca^{2+}, the percentage of WP3 cells attached to ferrihydrite particles was ca. 84% in one hour. Within the Ca-amended systems, the percent adhesion significantly increased to around 97%, regardless Ca^{2+} concentration.

3.3 Mineralogical, chemical and morphological analyses of solid products after bioreduction

3.3.1 XRD and ICP-OES

As shown in Figure 4, XRD patterns of the bioreduced products exhibited reflections of (012), (104), (110), (113), (202), (018) and (116) planes, which indicate the presence of the hexagonal (rhombohedral) structure. Specifically, the diffraction peaks of solid phases from the Ca-free biosystems matched well with those of siderite standard (PDF#29-0696) (Figure 4a), thus demonstrating that siderite was the major phase in these experiments. More interestingly, the XRD peaks of the solid products significantly shifted to lower 2θ values with increasing concentrations of Ca^{2+}, indicating the formation of Ca-Fe carbonates due to the incorporation of Ca^{2+} ions into siderite structure by replacing Fe^{2+} ions (Figure 4a). Additionally, it is shown that the reflection peaks of Ca-Fe carbonates from Ca-amended sets were broad, indicating that their crystal size is small and perhaps in the nanoscale range. The short XRD scans verified the downward shift of the (104) reflections (Figure 4b). Noticeably, the (104) peak position of the bioreduced product that was obtained from the 20 mmol/L Ca-amended bioreactors was close to that of the ankerite reference (PDF#41-0586) (Figure 4b), suggesting that this Ca-Fe carbonate neoformation had a chemical composition near that of theoretical

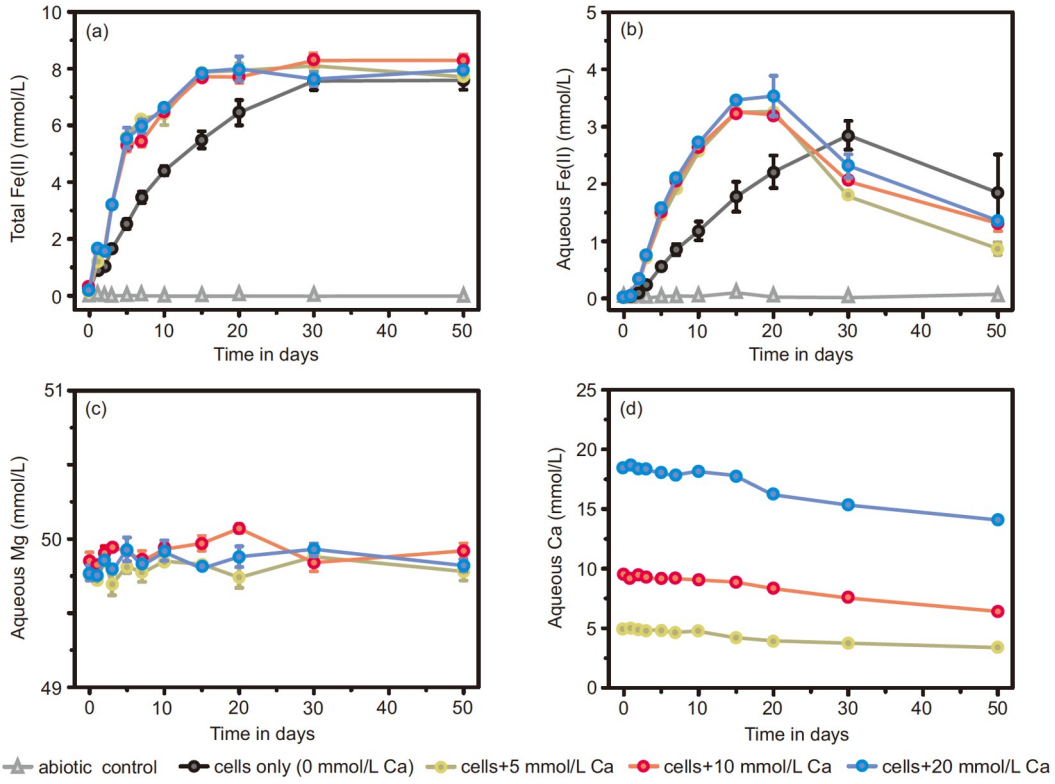

Figure 2 Time course change of concentration of total Fe(II) (a), aqueous Fe(II) (b), aqueous Mg (c) and aqueous Ca (d) during microbial iron reduction.

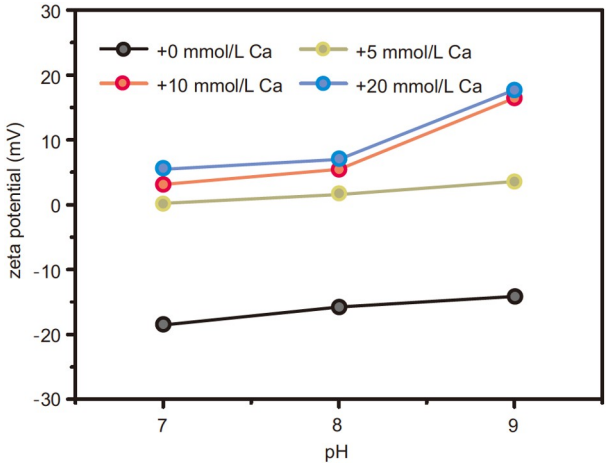

Figure 3 Zeta potential of ferrihydrite suspension in the presence of Ca^{2+} at different pHs. The plot shows systematically higher Zeta potentials for higher Ca^{2+} concentrations.

$CaFe(CO_3)_2$. However, the cation-ordering peaks [e.g., (101) and (015)] were absent in this ankerite-like phase, which suggests that the Ca-Fe arrangement of this mineral was disordered. The ICP-OES data indicated that the carbonates contained 0.03, 10.87, 17.51 and 39.65 mol% $CaCO_3$ from the bioreduction experiments with the starting Ca^{2+} concentrations of 0, 5, 10 and 20 mmol/L, respectively. Because of these chemical similarities, the term "proto-ankerite" is applied herein for biogenic ankerite-like mineral precipitates obtained from the 20 mmol/L Ca-amended biosystems.

A strong positive correlation was observed between the aforementioned ICP-OES data and the starting Ca^{2+} concentrations (Figure 5a). A similar positive correlation existed for the $CaCO_3$ content in the Ca-Fe carbonates with respect to the *d*-spacing values of (104) reflection (Figure 5b).

3.3.2 *Electron microscopic observations*

The TEM data revealed that biogenic siderite that formed from the Ca-free systems was 1–2 μm in size and well crystallized in euhedral structure (Figure 6a). Moreover, the corresponding EDS result confirmed the presence of $FeCO_3$ content. In contrast, the obtained Ca-Fe carbonates from the bioreactors with 5 and 10 mmol/L Ca^{2+} possessed coarse structures with a large number of nano-grains (Figure 6b–6e). Noticeably, the size of Ca-Fe carbonate that was collected from the 10 mmol/L Ca-amended systems (Figure 6e) was smaller than that from the 5 mmol/L experiments (Figure 6c). High-resolution TEM (HRTEM) image further revealed the dominant $d_{(104)}$ spacing of 0.283 nm for the Ca-Fe carbonate from the 10 mmol/L experiments (Figure 6f), consistent with the XRD data (Figure 5b). The presence of Ca was confirmed by EDS in these Ca-Fe carbonates (Figure 6c and 6g).

SEM observations of the bioreduced samples from the 20 mmol/L Ca experiments showed the WP3 cells in associated with proto-ankerite particles (Figure 7a). SEM and

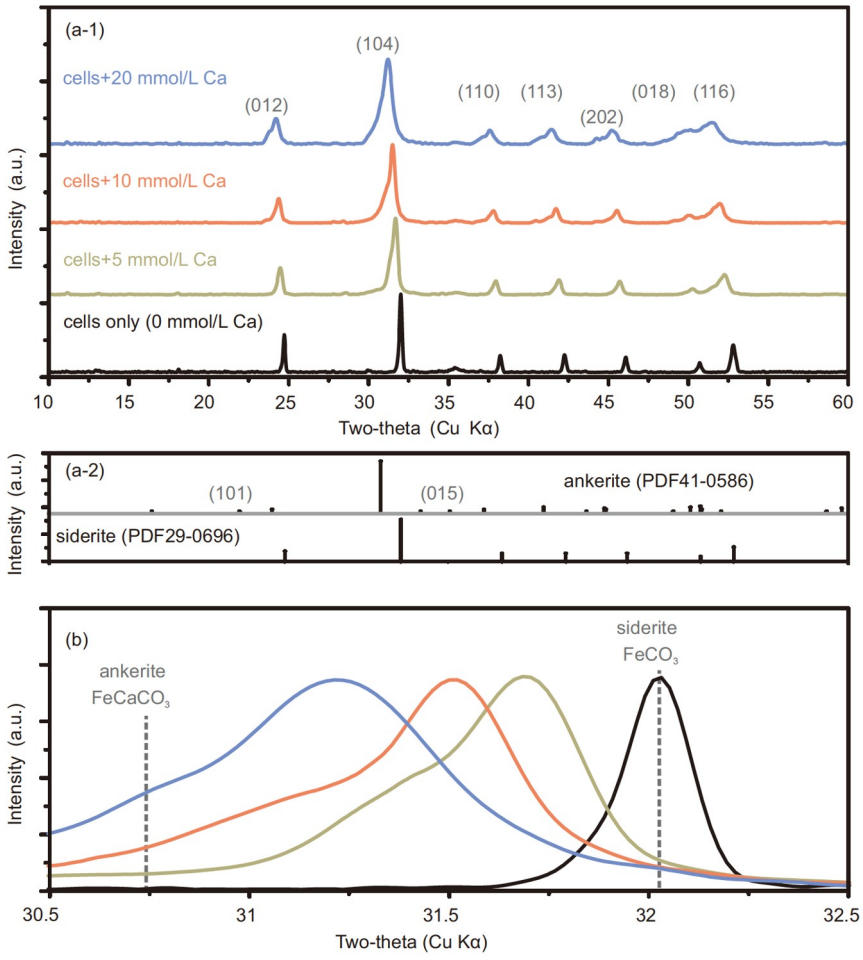

Figure 4 (a) Comparison XRD patterns (a-1) between secondary mineral products after 50 days of bioreduction and homogeneous in-house standards of iron-bearing minerals (ankerite and siderite) (a-2); (b) comparison of diagnostic XRD peaks in 2θ range of 30.5°–32.5° for the (104) plane. Note the broadening of peaks as well as their shift towards lower angles and smaller separation for experiments with higher Ca^{2+} concentrations.

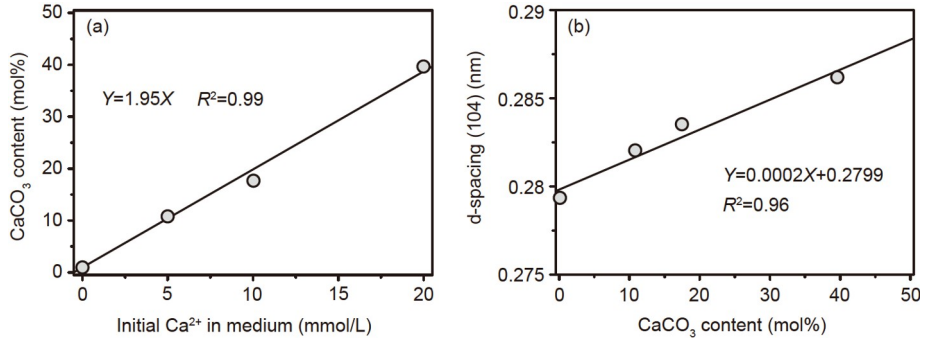

Figure 5 (a) Linear relationship between initial Ca^{2+} in medium and $CaCO_3$ content of Ca-Fe carbonate neoformations; (b) Relationship between $CaCO_3$ content of Ca-Fe carbonates and their $d_{(104)}$ values.

TEM data collectively revealed that the biogenic proto-ankerite was composed of numerous nano-spheres, with a mean size of 9 nm (Figure 7b–7e). As mentioned above, (101) and (015) are typical cation-ordering reflections for dolomite group minerals. The SAED pattern did not exhibit these superlattice reflections (Figure 7f), which supports the above XRD results. The proto-ankerite phase showed clear lattice fringes, and the width of the fringes was estimated to be 0.286 nm (Figure 7g). This data was in good agreement with the lattice spacing of the (104) plane revealed by XRD measurements (Figure 5b). EDS analyses indicated the signal level of Ca was nearly equal to that of Fe in proto-ankerite phases (Figure 7h). Moreover, a minor amount of Mg was also detected in EDS spectra (Figure 7h). The HRTEM data

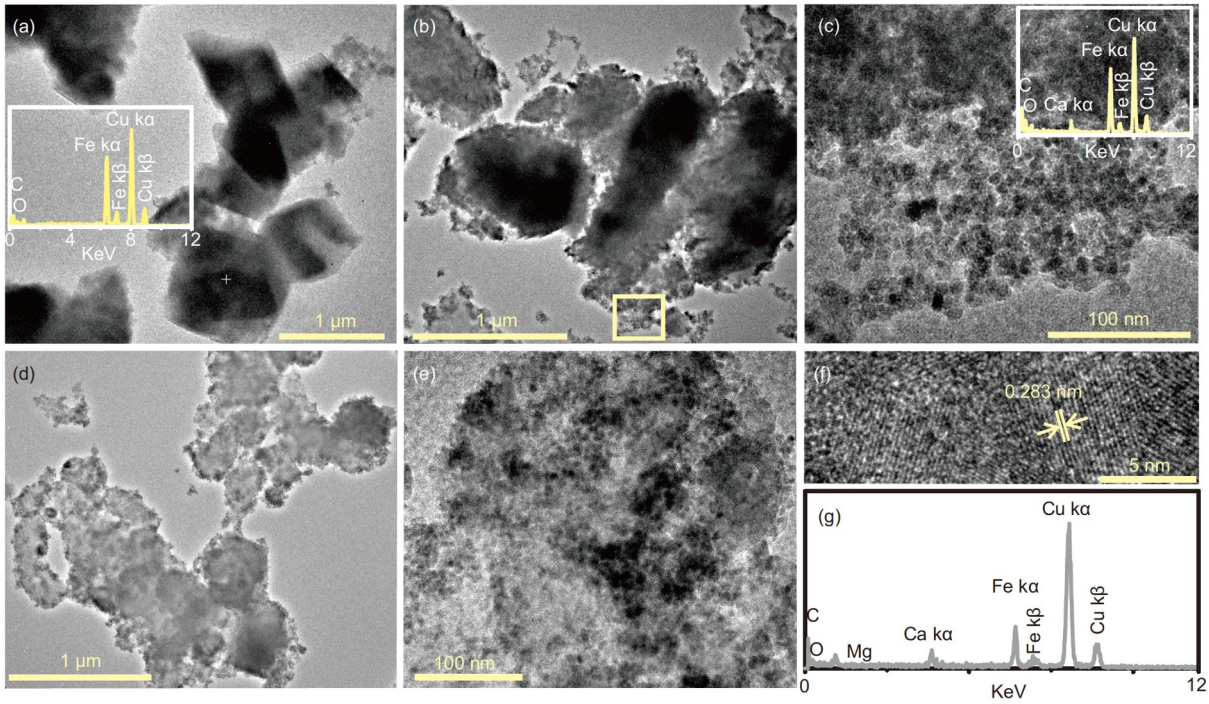

Figure 6 TEM images of secondary mineral products after bioreduction (day 50): (a) prismatic habit siderite produced in the Ca-free bioreactors. The insert EDS data shows the chemical composition of biogenic siderite, with contaminant Cu peaks from the TEM grid. (b) Anhedral Ca-Fe carbonates from the 5 mmol/L Ca-amended bioreactors. (c) An enlarged view of the square of B showing the nano-sized aggregates and their chemical composition. (d)–(g) The morphology, predominant lattice fringes, and chemical composition of Ca-Fe carbonates produced in the biosystems with 10 mmol/L Ca^{2+}.

also revealed that the proto-ankerite contained structural defects. Specifically, the (202) lattice fringes, identified with a *d*-spacing of 0.203 nm, were shown in Figure 8. Based on the inverse fast Fourier transformation (IFFT) analysis, a number of stacking faults were revealed within this biogenic mineral precipitate (Figure 8c).

3.4 Transformation of proto-ankerite into ankerite under hydrothermal conditions

After hydrothermal alteration of proto-ankerite in a Mg/Ca saline solution, XRD data showed that the main solid phase was ankerite, along with minor siderite (Figure 9a). In comparison to proto-ankerite, ankerite exhibited significantly sharper XRD peaks and distinctive characteristic reflections of (101), (015) and (021). The ankerite neoformation was blocky and densely packed, and grain size ranged homogeneously between 140 and 170 nm (Figure 9b). As evidenced by EDS, ankerite contained also significant amounts of Mg, Ca and Fe (Figure 9b). ICP-OES measurements can provide more accurate information about the mineral composition. The ICP-OES data indicated that our ankerite sample was composed of 49.8 mol% $CaCO_3$, 27.2 mol% $FeCO_3$, and 23 mol% $MgCO_3$. Therefore, its structural formula can be expressed as $CaFe_{0.54}Mg_{0.46}(CO_3)_2$, which is quite close to the ankerite composition [$CaMg_{0.5}Fe_{0.5}(CO_3)_2$] defined by IMA.

4. Discussion

4.1 Effect of Ca^{2+} on microbial reduction of ferrihydrite

Owing to the fact that ferric iron [Fe(III)] is essentially insoluble in neutral pH environments, DIRB face the problem of transferring electrons extracellularly to Fe(III) minerals outside of their cells (Shi et al., 2016). Although DIRB have evolved multiple strategies for utilizing such low solubility electron acceptors, it is a consensus that microbial reduction of Fe(III) minerals is a rate-limiting process, and that the rate of microbial reduction of solid Fe(III) phases can be influenced by a great variety of factors (Roden, 2004; Bonneville et al., 2009). For instance, mineral surface area, particle size and crystallinity have been identified as major mineralogical factors controlling the initial rate of microbial iron reduction (Roden, 2004; Bose et al., 2009; Liu et al., 2012). In addition to mineralogical factors, several geochemical factors are reported to govern the kinetics of microbial reduction of Fe (III) minerals. For example, a quinone-containing compound is known to serve as an electron shuttle to promote microbial iron reduction (Lovley et al., 1996).

In the present study, we demonstrated that the presence of Ca^{2+} could accelerate the bioreduction rate with strain WP3 (Figure 2a). Apparently, Ca^{2+} ion lacks the electron shuttling capability, so there should be some other mechanisms involving the positive effect of Ca^{2+}. It is well documented that

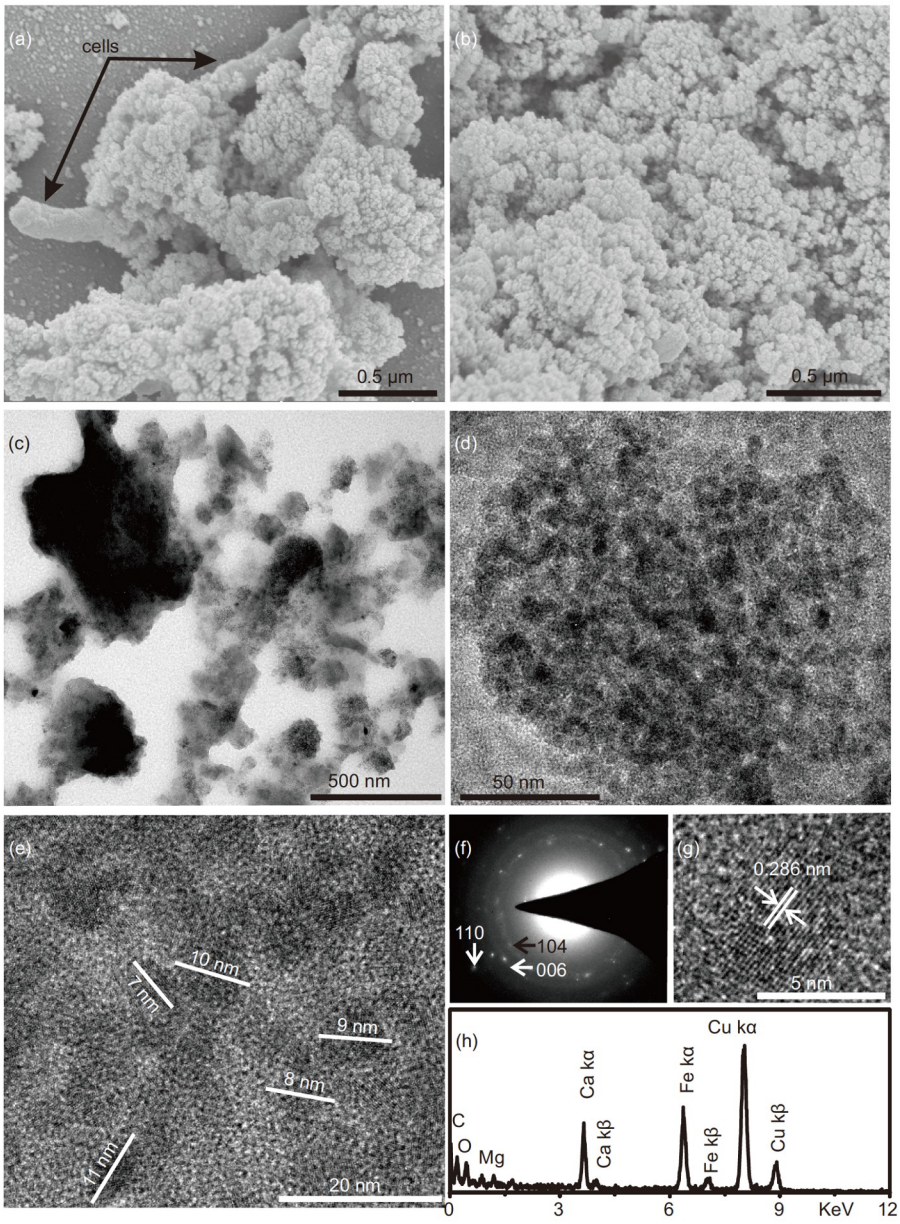

Figure 7 SEM (a)–(b) and TEM (c)–(h) images of proto-ankerite nanoparticle collected by the end of experiments (50 days) from the bioreactors with 20 mmol/L Ca^{2+}.

in the absence of exogenous electron shuttles, DIRB (e.g., *Shewanella* spp.) primarily employ the mechanism of direct cell-mineral contact to transfer extracellular electrons (Bose et al., 2009). Therefore, the adhesion efficiency of DIRB cells with Fe(III) minerals plays a vital role in the bioreduction of Fe(III). Indeed, an experimental study by O'Loughlin et al. (2010) demonstrated that the bioreduction of lepidocrocite was inhibited by phosphate, silicate, and other inorganic oxyanions, due to the competitive adsorption of oxyanions onto lepidocrocite surfaces which can block the access of bacterial cells and reduce bacterial adhesion.

Microbial adhesion to mineral surfaces is, at least in part, regulated by electrostatic force (Yee et al., 2000). Normally ferrihydrite is positively charged. However, our Ca-free ferrihydrite suspension had a negative potential (Figure 3), indicating that the ferrihydrite surface developed a net negative charge. This phenomenon might be explained by the coating effect of organic molecules from yeast extract. Due to the existence of a high density of ferric hydroxyl functional groups (≡FeOH) on the surface of ferrihydrite, this mineral has a high adsorption capacity for organic molecules (Eusterhues et al., 2011). Noticeably, the microbial cell surface is often negatively charged owing to the presence of acidic functional groups such as carboxyl, hydroxyl, and phosphate (Yee et al., 2000). In this regard, a repulsive force existed when WP3 cells interacted with ferrihydrite particles

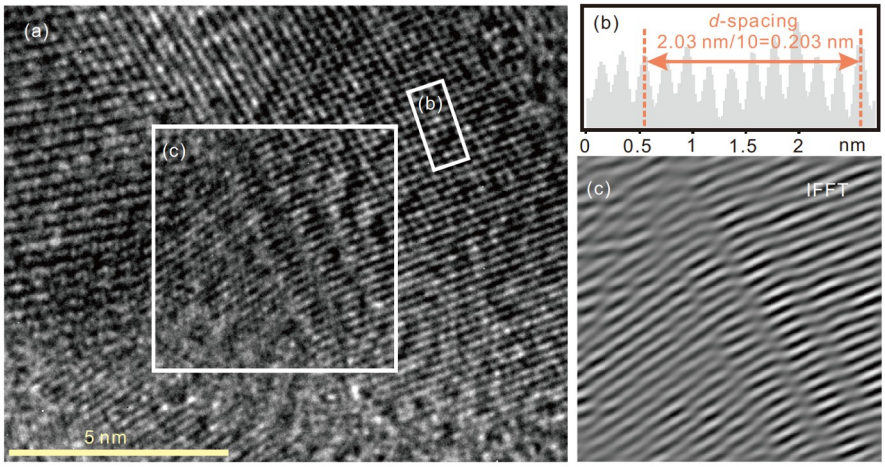

Figure 8 (a) HRTEM image showing the lattice fringes of microbially-induced proto-ankerite obtained after the bioreduction systems for 50 days; (b) the lattice spacing distribution of the selected area in the panel (a); (c) the inverse FFT of the square area in the panel (a) showing the stacking faults.

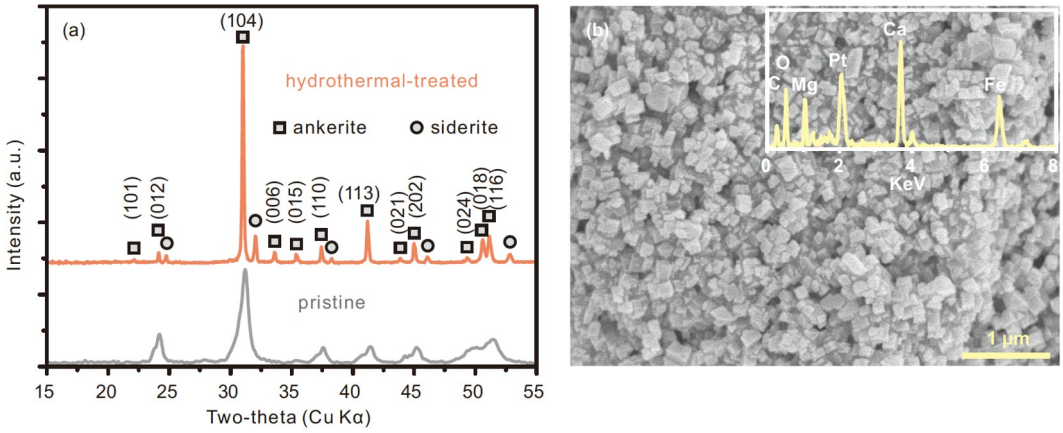

Figure 9 (a) XRD results showing the differences between pristine and hydrothermal-treated proto-ankerite, where the peaks in the pristine proto-ankerite are significantly broader than in the hydrothermal experiment; (b) SEM image and EDS data of ordered ankerite from a two-month hydrothermal experiments.

in our systems, which potentially limited the adhesion efficiency and bioreduction rate. When Ca^{2+} ions were introduced into the bioreduction systems, ≡FeOH groups of ferrihydrite could also coordinate with Ca^{2+} ions forming $\equiv[(FeOH)_2Ca]^{2+}$ complexes (Mendez and Hiemstra, 2020). As such, ferrihydrite dispersion tended to become positively charged in the presence of Ca^{2+}, which is validated by its positive zeta potential values (Figure 3). In doing so, an electrostatic attraction between WP3 cells and ferrihydrite particles could occur in the presence of Ca^{2+}, which might account for the enhanced reduction rate in these Ca-amended bio-systems. Although zeta potentials of ferrihydrite suspension gradually increased with increasing Ca concentrations (0–20 mmol/L), almost all of the WP3 cells were already adhered to ferrihydrite in the Ca-amended systems. These adhesion data can interpret the similar bioreduction rates observed in Ca-amended systems (Figure 2a).

The final extents of Fe(III) reduction for the bioreactors were in the range of 76.4–83.5%. These data demonstrated that the bioreduction of ferrihydrite by strain WP3 was an incomplete process. Owing to excessive lactate used in our experiments, this incomplete bioreduction was not the result of insufficient electron donation. In fact, similar results have been observed for other DIRB such as *S. putrefaciens* CN32 (Fredrickson et al., 1998) and *S. oneidensis* MR-1 (Amstaetter et al., 2012). According to previous experimental studies, the incomplete bioreduction of Fe(III)-containing minerals is mainly ascribed to the blocking effect of produced Fe(II) (Roden and Urrutia, 1999; Urrutia et al., 1999). During bioreduction, a considerable amount of Fe(II) ions can be released into aqueous solutions (Figure 2b). These produced Fe(II) ions are preferentially adsorbed onto Fe(III)-containing minerals and cell surfaces, leading to the blockage of active surface sites (Roden and Urrutia, 1999). In addition, mineral aggregation has also been thought to inhibit long-term bioreduction (Urrutia et al., 1999). As evidenced by our microscopic data, the neoformed Ca-Fe carbonates were shown to be in aggregate form (Figures 6 and 7). No-

ticeably, WP3 cells were embedded in the neoformed aggregates (Figure 7a). It is reasonable to speculate that the Ca-Fe carbonate neoformations might physically block the microbial extracellular electron transfer.

4.2 Formation mechanism of Ca-Fe carbonate mediated by *S. piezotolerans* WP3

It has been well documented that microbial reduction of Fe(III) oxides can result in the formation of secondary Fe(II)-bearing minerals, such as siderite, vivianite, magnetite, and green rust (Fredrickson et al., 1998; Ona-Nguema et al., 2002; O'Loughlin et al., 2010; Wu et al., 2011). The rate of Fe(II) production and aqueous chemical composition are two crucial parameters in regulating the crystallization of specific Fe(II) phases (Fredrickson et al., 1998; O'Loughlin et al., 2010). Specifically for siderite, it is a common mineral product observed in the bioreduction systems with a high production rate of Fe(II) and high alkalinity (Fredrickson et al., 1998). In the present study, the medium used for bioreduction experiments contained high amounts of dissolved inorganic carbon (DIC; 30 mmol/L HCO_3^-). Microbial mineralization of organic sources of carbon (e.g., lactate used herein) can also enhance the concentration of DIC. Furthermore, as evidenced by ammonium production (Figure 1), strain WP3 had the ability to ammonify the nitrogen sources in yeast extract. Specifically, only a slight rise in pH was observed for the abiotic reactors (Figure 1a), which might be caused by the protonation of hydroxyl and (or) carboxyl sites within yeast extract. However, sharper increases in pH as well as alkalinity occurred in the bioreactors (Figure 1a). These significant changes observed in the bioreduction systems might be attributed to microbial ammonification (yeast extract$\rightarrow NH_3+H_2O\rightarrow NH_4^+ + OH^-$). Taken together, the concentration of CO_3^{2-} could be significantly elevated due to DIC partitioning under an alkaline environment, thus providing oversaturated conditions for siderite when Fe^{2+} ions were present in aqueous solutions (Figure 2). Aforementioned results can explain the occurrence of siderite in our Ca-free systems.

When Ca^{2+} ions were introduced in our bioreduction systems, Ca-Fe carbonate neoformations occurred and their $CaCO_3$ content was highly dependent on the starting concentration of Ca^{2+} in solutions. Given the fact that the charge density and ionic radius of Ca^{2+} are similar to those of Fe^{2+}, the Fe^{2+} sites in the lattice of siderite can be theoretically substituted by Ca^{2+} ions (Romanek et al., 2009). Indeed, cation-disordered phases in the (Ca,Fe)CO_3 have been successfully synthesized at low temperatures. For instance, Romanek et al. (2009) reported that the Ca-Fe carbonates that were inorganically synthesized at 25°C had the $CaCO_3$ content less than 17 mol% (Romanek et al., 2009). Our present study showed that strain WP3 was capable of facilitating the loading of Ca^{2+} during Ca-Fe carbonate growth at 20°C. The $CaCO_3$ content of our Ca-Fe carbonates was estimated up to 39.65 mol%. This value is much higher than that of low-temperature inorganic counterparts mentioned above. Such apparent discrepancy might be attributed to the high aqueous Ca/Fe ratio observed in our bioreduction systems. Specifically, the Ca/Fe molar ratio of experimental solutions using by Romanek et al. (2009) was within the range of 0.03–1.05. Although the concentrations of aqueous Fe(II) in all bioreactors increased as a consequence of microbial reduction of ferrihydrite (Figure 2b), the average Ca/Fe molar ratio was still as high as 8.36, 14.09 and 28.65 for the bioreactors with 5, 10 and 20 mmol/L Ca^{2+}, respectively. Apparently, a solution with high Ca/Fe ratios can provide sufficient Ca^{2+} for the growth of Ca-Fe carbonates.

It is relevant to note that both Ca^{2+} and Fe^{2+} are typically hydrated in solutions (Lippmann, 1973). As such, there exists an energy barrier against the hydration shell of these cations, blocking the approach of CO_3^{2-} ions to either Ca^{2+} or Fe^{2+} ions. This hydration effect can be diminished at high temperature when the thermal energy exceeds the energy barrier variations, whereas it persists at ambient temperature (Romanek et al., 2009). The occurrence of low-temperature biogenic Ca-Fe carbonates showed that strain WP3 had a positive effect on dehydration of Ca^{2+} and Fe^{2+}. Actually, the catalytic role of microorganisms in the dehydration of metal ions has been long recognized and interpreted as suggesting that the negatively-charged groups (especially carboxyl) on microbial cells break down the hydration shell of metal ions via electrostatic forces (de Vasquez et al., 2021). In general, carboxyl and other acidic groups preferentially interact with metal ions to form cation-organic complexes, accompanied by the partial removal of the outer shell water around the metal cations (Qiu et al., 2017; Huang et al., 2019). According to the study reported by Huang et al. (2019), strain WP3 has a high density of cell surface-bound carboxyl groups (0.057/Å^2), which is significantly higher than non-marine DIRB (0.03/Å^2) (Kenward et al., 2013). Therefore, it is reasonable to speculate that WP3 cells can lower the energy barrier to the incorporation of Ca^{2+} and Fe^{2+} into growing Ca-Fe carbonates.

Besides Ca ions, our bioreduction medium also contained considerable amounts of Mg^{2+}. However, as evidenced by the new EDS data, only trace amounts of Mg were detected in the Ca-Fe carbonates (Figure 7h), which is consistent with a previous study that showed the formation of a (Ca,Fe)CO_3 phase rather than (Ca,Mg,Fe)CO_3 in bioreduced systems with ferric hydroxide, a non-marine DIRB (*S. oneidensis* MR-1), as well as Ca^{2+} and Mg^{2+} ions (Zeng and Tice, 2014). Thus, these results demonstrate that Ca^{2+} is more effective than Mg^{2+} in competing for the substitution of Fe. Such

phenomenon is likely accounted for by the difference in dehydration enthalpy of Ca^{2+} vs. Mg^{2+}. Numerous computational studies have demonstrated that Mg^{2+} has the higher dehydration enthalpy than Ca^{2+} (351.8 kcal/mole vs. 264.3 kcal/mole) (Jiao et al., 2006), owing to longer lifetime of water molecules around Mg^{2+} and higher surface charge density of this cation (Jiao et al., 2006; Romanek et al., 2009). As a result, more energy is required for the dissociation of Mg-H_2O complexes compared to Ca-H_2O complexes, and thus Mg incorporation in the Ca-Fe carbonate structure is quite limited at low temperature.

4.3 Proto-ankerite and its transformation

The Ca-Fe carbonate produced from the 20 mmol/L Ca-amended bioreactors had an average $CaCO_3$ content of 39.65 mol%, that is, with a chemical formula of $Ca_{0.8}Fe_{1.2}(CO_3)_2$. This chemical composition is close to that of "theoretical" ankerite [$CaFe(CO_3)_2$]. However, as mentioned earlier, our ankerite-like neoformation lacked Ca-Fe ordering as evidenced by XRD and SAED data. Not limited to aforementioned ankerite-like phase, the synthesis of other disordered double carbonates has also been achieved under ambient conditions due to the presence of microbial activity. Disordered dolomite is a good example with new recent advances. A growing number of studies reveal that various types of microbes can facilitate the precipitation of Ca-Mg carbonates at Earth surface temperatures (e.g., Vasconcelos et al., 1995; Sánchez-Román et al., 2008; Bontognali et al., 2012; Qiu et al., 2017; Huang et al., 2019; Liu D et al., 2019, 2020; Zhang et al., 2021; Han et al., 2022). The Mg level of these microbially-induced Ca-Mg carbonates is generally above 10 mol% and reaches up to 48 mol%. According to the definition of Graf and Goldsmith (1956), the Ca-Mg carbonate having near-dolomite stoichiometry (≥36 mol% $MgCO_3$) but disordered Ca-Mg arrangement should be termed "proto-dolomite". A number of laboratory experiments have demonstrated that proto-dolomite can convert into dolomite during burial diagenesis (Malone et al., 1996; Rodriguez-Blanco et al., 2015; Kaczmarek and Thornton, 2017; Zheng et al., 2021). Motivated by these studies, herein we introduce the term "proto-ankerite" to describe Ca-Fe carbonate which is of approximately ankeritic composition but lacks Ca-Fe order.

It is a general consensus that nanominerals are highly reactive due to their high surface-to-volume ratio (Hochella Jr. et al., 2008). Our proto-ankerites were in the range of a few nanometers (Figure 7). It has been also reported that some microbially-mediated minerals (e.g., ZnS) have much more defective crystalline structures compared to their abiotic counterparts (e.g., Xu et al., 2016). In the new experiments, TEM data revealed that planar defects were also present in low-temperature proto-ankerite (Figure 8). These nano-scale and defect-rich properties should allow microbially-induced ankerite to be unstable in open diagenetic environments where intense alterations triggered by external fluid take place. Indeed, our hydrothermal experiments showed that the proto-ankerite was converted into ankerite at 100°C in a Mg/Ca-containing saline solution, demonstrating that microbially-mediated proto-ankerite can serve as a precursor for sedimentary ankerite. Unlike Mg-poor nature of proto-ankerite, the newly-formed ankerite had equal amounts of Mg and Fe (Figure 9b). These results suggested that high temperatures can lower the activation barrier for Mg^{2+} dehydration and that Mg incorporation in ankerite is achieved by the substitution of Mg for Fe. Indeed, siderite was found to accompany the hydrothermal transformation of proto-ankerite to ankerite (Figure 9a), which can serve as indirect evidence for the release of Fe^{2+} from proto-ankerite due to Mg substitution.

Many ankerite cements are commonly found in shallow marine sandstone reservoirs (e.g., Kantorowicz, 1985; Hendry et al., 2000), and most were thought to be early diagenetic and authigenic in origin (Kantorowicz, 1985). It is noted that those ankerite cements had negative $\delta^{13}C$ values. For instance, ankerite cements from the Wilcox Group in southwest Texas had $\delta^{13}C$ values from −5.2‰ to −9.0‰ PDB (Kantorowicz, 1985). These $\delta^{13}C$ signatures may be related to the microbial oxidation of organic substrates. Moreover, siderite was frequently observed to co-exist with ankerite in aforementioned settings. On the basis of our cultivation and precipitation experiments, as well as published field studies, we propose that microbial iron reduction can contribute to the genesis of sedimentary ankerite (Figure 10). Similar to the recognized mediation of microorganisms in the precipitation of dolomite, microorganisms facilitate the formation of ankerite by providing a metastable, low-temperature carbonate precursor, which can be converted into ordered counterpart upon diagenesis and hydrothermal alteration.

5. Conclusions

Through laboratory experiments we demonstrated the formation of Ca-Fe carbonates from bioreduction of ferrihydrite by *S. piezotolerans* WP3 in a bicarbonate-buffered, Ca^{2+}-amended medium. The content of $CaCO_3$ in the neoformed Ca-Fe carbonates was positively correlated with the initial concentration of Ca^{2+} within the medium. Microbially-induced proto-ankerite having 39.65 mol% $CaCO_3$ was observed when the concentration of Ca^{2+} was up to 20 mmol/L. Our proto-ankerite was nanoscopic in size, spherical in shape, cation-disordered, and with a defective crystalline structure. The hydrothermal experiments provided evidence that ordered ankerite can be produced through the recrystallization of biogenic proto-ankerite at 100°C. The

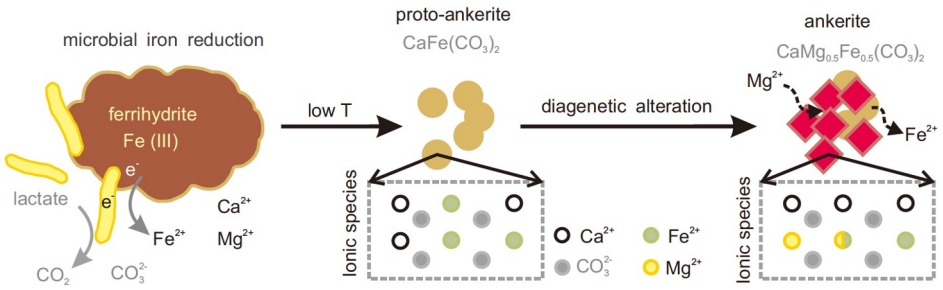

Figure 10 Proposed model illustrating the role of iron-reducing microbes on the formation of ankerite.

conversion of proto-ankerite to ankerite was triggered by the substitution of Mg^{2+} for Fe^{2+} in the lattice structure, leading to solubilization of excess Fe and concomitant siderite precipitation.

Acknowledgements *The authors are grateful to the handling editor and two anonymous reviewers whose comments improved the quality of this manuscript. This research was jointly supported by the National Natural Science Foundation of China (Grant Nos. 42272046, 42293292 and 42072336), the National Key R&D Program of China (Grant No. 2022YFF0800304), and the 111 Project (Grant No. BP0820004).*

Conflict of interest The authors declare that they have no conflict of interest.

References

Amstaetter K, Borch T, Kappler A. 2012. Influence of humic acid imposed changes of ferrihydrite aggregation on microbial Fe(III) reduction. Geochim Cosmochim Acta, 85: 326–341

Bonneville S, Behrends T, Van Cappellen P. 2009. Solubility and dissimilatory reduction kinetics of iron(III) oxyhydroxides: A linear free energy relationship. Geochim Cosmochim Acta, 73: 5273–5282

Bontognali T R R, Vasconcelos C, Warthmann R J, Lundberg R, McKenzie J A. 2012. Dolomite-mediating bacterium isolated from the sabkha of Abu Dhabi (UAE). Terra Nova, 24: 248–254

Bose S, Hochella Jr. M F, Gorby Y A, Kennedy D W, McCready D E, Madden A S, Lower B H. 2009. Bioreduction of hematite nanoparticles by the dissimilatory iron reducing bacterium *Shewanella oneidensis* MR-1. Geochim Cosmochim Acta, 73: 962–976

Chang B, Li C, Liu D, Foster I, Tripati A, Lloyd M K, Maradiaga I, Luo G, An Z, She Z, Xie S, Tong J, Huang J, Algeo T J, Lyons T W, Immenhauser A. 2020. Massive formation of early diagenetic dolomite in the Ediacaran ocean: Constraints on the "dolomite problem". Proc Natl Acad Sci USA, 117: 14005–14014

de Vasquez M G V, Rudd B A W, Baer M D, Beasley E E, Allen H C. 2021. Role of hydration in magnesium versus calcium ion pairing with carboxylate: Solution and the aqueous interface. J Phys Chem B, 125: 11308–11319

Eusterhues K, Rennert T, Knicker H, Kögel-Knabner I, Totsche K U, Schwertmann U. 2011. Fractionation of organic matter due to reaction with ferrihydrite: Coprecipitation versus adsorption. Environ. Environ Sci Technol, 45: 527–533

Fredrickson J K, Zachara J M, Kennedy D W, Dong H, Onstott T C, Hinman N W, Li S. 1998. Biogenic iron mineralization accompanying the dissimilatory reduction of hydrous ferric oxide by a groundwater bacterium. Geochim Cosmochim Acta, 62: 3239–3257

Graf D L, Goldsmith J R. 1956. Some hydrothermal syntheses of dolomite and protodolomite. J Geol, 64: 173–186

Gregg J M, Bish D L, Kaczmarek S E, Machel H G. 2015. Mineralogy, nucleation and growth of dolomite in the laboratory and sedimentary environment: A review. Sedimentology, 62: 1749–1769

Guo C, Chen D Z, Dong S F, Qian Y X, Liu C G. 2017. Early dolomitisation of the Lower-Middle Ordovician cyclic carbonates in northern Tarim Basin, NW China. Sci China Earth Sci, 60: 1283–1298

Han Z, Qi P, Zhao Y, Guo N, Yan H, Tucker M E, Li D, Wang J, Zhao H. 2022. High Mg/Ca molar ratios promote protodolomite precipitation induced by the extreme halophilic bacterium *Vibrio harveyi* QPL$_2$. Front Microbiol, 13: 821968

Hendry J P, Wilkinson M, Fallick A E, Haszeldine R S. 2000. Ankerite cementation in deeply buried Jurassic sandstone reservoirs of the central North Sea. J Sediment Res, 70: 227–239

Higgins J A, Blättler C L, Lundstrom E A, Santiago-Ramos D P, Akhtar A A, Crüger Ahm A S, Bialik O, Holmden C, Bradbury H, Murray S T, Swart P K. 2018. Mineralogy, early marine diagenesis, and the chemistry of shallow-water carbonate sediments. Geochim Cosmochim Acta, 220: 512–534

Hochella Jr. M F, Lower S K, Maurice P A, Penn R L, Sahai N, Sparks D L, Twining B S. 2008. Nanominerals, mineral nanoparticles, and Earth systems. Science, 319: 1631–1635

Huang Y R, Yao Q Z, Li H, Wang F P, Zhou G T, Fu S Q. 2019. Aerobically incubated bacterial biomass-promoted formation of disordered dolomite and implication for dolomite formation. Chem Geol, 523: 19–30

Jiao D, King C, Grossfield A, Darden T A, Ren P. 2006. Simulation of Ca^{2+} and Mg^{2+} solvation using polarizable atomic multipole potential. J Phys Chem B, 110: 18553–18559

Kaczmarek S E, Thornton B P. 2017. The effect of temperature on stoichiometry, cation ordering, and reaction rate in high-temperature dolomitization experiments. Chem Geol, 468: 32–41

Kantorowicz J D. 1985. The origin of authigenic ankerite from the Ninian Field, UK North Sea. Nature, 315: 214–216

Kenward P A, Fowle D A, Goldstein R H, Ueshima M, González L A, Roberts J A. 2013. Ordered low-temperature dolomite mediated by carboxyl-group density of microbial cell walls. AAPG Bull, 97: 2113–2125

Li M, Wignall P B, Dai X, Hu M, Song H. 2021. Phanerozoic variation in dolomite abundance linked to oceanic anoxia. Geology, 49: 698–702

Lippmann F. 1973. Crystal chemistry of sedimentary carbonate minerals. In: Sedimentary Carbonate Minerals. Berlin: Springer. 5–96

Liu C, Li W. 2020. Transformation of amorphous precursor to crystalline carbonate: Insights from Mg isotopes in the dolomite-analogue mineral norsethite [$BaMg(CO_3)_2$]. Geochim Cosmochim Acta, 272: 1–20

Liu D, Dong H, Bishop M E, Zhang J, Wang H, Xie S, Wang S, Huang L, Eberl D D. 2012. Microbial reduction of structural iron in interstratified illite-smectite minerals by a sulfate-reducing bacterium. Geobiology, 10: 150–162

Liu D, Fan Q, Papineau D, Yu N, Chu Y, Wang H, Qiu X, Wang X. 2020. Precipitation of protodolomite facilitated by sulfate-reducing bacteria: The role of capsule extracellular polymeric substances. Chem Geol, 533: 119415

Liu D, Yu N, Papineau D, Fan Q, Wang H, Qiu X, She Z, Luo G. 2019. The

catalytic role of planktonic aerobic heterotrophic bacteria in proto-dolomite formation: Results from Lake Jibuhulangtu Nuur, Inner Mongolia, China. Geochim Cosmochim Acta, 263: 31–49
Liu Y, Chen C, He D, Chen W. 2019. Deep carbon cycle in subduction zones. Sci China Earth Sci, 62: 1764–1782
Lovley D R, Coates J D, Blunt-Harris E L, Phillips E J P, Woodward J C. 1996. Humic substances as electron acceptors for microbial respiration. Nature, 382: 445–448
Malone M J, Baker P A, Burns S J. 1996. Recrystallization of dolomite: An experimental study from. Geochim Cosmochim Acta, 60: 2189–2207
Marin F, Smith M, Isa Y, Muyzer G, Westbroek P. 1996. Skeletal matrices, muci, and the origin of invertebrate calcification.. Proc Natl Acad Sci USA, 93: 1554–1559
McLeod S. 1992. Micro-distillation unit for use in continuous flow analyzers. Its construction and use in determination of ammonia and nitrate in soils. Anal Chim Acta, 266: 107–112
Mendez J C, Hiemstra T. 2020. Ternary complex formation of phosphate with Ca and Mg ions binding to ferrihydrite: Experiments and mechanisms. ACS Earth Space Chem, 4: 545–557
O'Loughlin E J, Gorski C A, Scherer M M, Boyanov M I, Kemner K M. 2010. Effects of oxyanions, natural organic matter, and bacterial cell numbers on the bioreduction of lepidocrocite (γ-FeOOH) and the formation of secondary mineralization products. Environ Sci Technol, 44: 4570–4576
Ona-Nguema G, Abdelmoula M, Jorand F, Benali O, Antoine Géhin, O, Block J C, Génin J M R. 2002. Iron (II, III) hydroxycarbonate green rust formation and stabilization from lepidocrocite bioreduction. Environ Sci Technol, 36: 16–20
Perri E, Tucker M. 2007. Bacterial fossils and microbial dolomite in Triassic stromatolites. Geology, 35: 207–210
Petrash D A, Bialik O M, Bontognali T R R, Vasconcelos C, Roberts J A, McKenzie J A, Konhauser K O. 2017. Microbially catalyzed dolomite formation: From near-surface to burial. Earth-Sci Rev, 171: 558–582
Pimentel C, Pina C M. 2016. Reaction pathways towards the formation of dolomite-analogues at ambient conditions. Geochim Cosmochim Acta, 178: 259–267
Qiu X, Wang H, Yao Y, Duan Y. 2017. High salinity facilitates dolomite precipitation mediated by *Haloferax volcanii* DS52. Earth Planet Sci Lett, 472: 197–205
Roden E E, Leonardo M R, Ferris F G. 2002. Immobilization of strontium during iron biomineralization coupled to dissimilatory hydrous ferric oxide reduction. Geochim Cosmochim Acta, 66: 2823–2839
Roden E E, Urrutia M M. 1999. Ferrous iron removal promotes microbial reduction of crystalline iron(III) oxides. Environ Sci Technol, 33: 1847–1853
Roden E E. 2004. Analysis of long-term bacterial vs. chemical Fe(III) oxide reduction kinetics. Geochim Cosmochim Acta, 68: 3205–3216
Rodriguez-Blanco J D, Shaw S, Benning L G. 2015. A route for the direct crystallization of dolomite. Am Mineral, 100: 1172–1181
Romanek C S, Jiménez-López C, Navarro A R, Sánchez-Román M, Sahai N, Coleman M. 2009. Inorganic synthesis of Fe–Ca–Mg carbonates at low temperature. Geochim Cosmochim Acta, 73: 5361–5376
Sánchez-Román M, Vasconcelos C, Schmid T, Dittrich M, McKenzie J A, Zenobi R, Rivadeneyra M A. 2008. Aerobic microbial dolomite at the nanometer scale: Implications for the geologic record. Geology, 36: 879
Sarazin G, Michard G, Prevot F. 1999. A rapid and accurate spectroscopic method for alkalinity measurements in sea water samples. Water Res, 33: 290–294
Schrag D P, Higgins J A, Macdonald F A, Johnston D T. 2013. Authigenic carbonate and the histroy of the global carbon cycle. Science, 339: 540–543
Schwertmann U, Cornell R M. 1991. Iron Oxides in the Laboratory: Preparation and Characterization. New York: VCH Publishers, Inc
Shi L, Dong H, Reguera G, Beyenal H, Lu A, Liu J, Yu H Q, Fredrickson J K. 2016. Extracellular electron transfer mechanisms between microorganisms and minerals. Nat Rev Microbiol, 14: 651–662
Stookey L L. 1970. Ferrozine—A new spectrophotometric reagent for iron. Anal Chem, 42: 779–781
Urrutia M M, Roden E E, Zachara J M. 1999. Influence of aqueous and solid-phase Fe(II) complexants on microbial reduction of crystalline iron(III) oxides. Environ Sci Technol, 33: 4022–4028
Vasconcelos C, McKenzie J A, Bernasconi S, Grujic D, Tiens A J. 1995. Microbial mediation as a possible mechanism for natural dolomite formation at low temperatures. Nature, 377: 220–222
Wang F, Wang J, Jian H, Zhang B, Li S, Wang F, Zeng X, Gao L, Bartlett D H, Yu J, Hu S, Xiao X. 2008. Environmental adaptation: Genomic analysis of the piezotolerant and psychrotolerant deep-sea iron-reduing bacterium *Shewanella piezotolerans* WP3. Plos One, 3: 1–12
Wen Y, Sánchez-Román M, Li Y, Wang C, Han Z, Zhang L, Gao Y. 2020. Nucleation and stabilization of Eocene dolomite in evaporative lacustrine deposits from central Tibetan plateau. Sedimentology, 67: 3333–3354
Wu W, Li B, Hu J, Li J, Wang F, Pan Y. 2011. Iron reduction and magnetite biomineralization mediated by a deep-sea iron-reducing bacterium *Shewanella piezotolerans* WP3. J Geophys Res, 116: G04034
Xie S C, Liu D, Qiu X, Huang X Y, Algeo T J. 2016. Microbial roles equivalent to geological agents of high temperature and pressure in deep Earth. Sci China Earth Sci, 59: 2098–2104
Xu F, You X, Li Q, Liu Y. 2019. Can primary ferroan dolomite and ankerite be precipitated? Its implications for formation of submarine methane-derived authigenic carbonate (MDAC) chimney. Minerals, 9: 413
Xu J, Murayama M, Roco C M, Veeramani H, Michel F M, Rimstidt J D, Winkler C, Hochella Jr. M F. 2016. Highly-defective nanocrystals of ZnS formed via dissimilatory bacterial sulfate reduction: A comparative study with their abiogenic analogues. Geochim Cosmochim Acta, 180: 1–14
Yee N, Fein J B, Daughney C J. 2000. Experimental study of the pH, ionic strength, and reversibility behavior of bacteria-mineral adsorption. Geochim Cosmochim Acta, 64: 609–617
You X L, Sun S, Zhu J Q. 2014. Significance of fossilized microbes from the Cambrian stromatolites in the Tarim Basin, Northwest China. Sci China Earth Sci, 57: 2901–2913
Zeng Z, Tice M M. 2014. Promotion and nucleation of carbonate precipitation during microbial iron reduction. Geobiology, 12: 362–371
Zhang F, Xu H, Konishi H, Shelobolina E S, Roden E E. 2012. Polysaccharide-catalyzed nucleation and growth of disordered dolomite: A potential precursor of sedimentary dolomite. Am Mineral, 97: 556–567
Zhang F, Xu H, Shelobolina E S, Konishi H, Roden E E. 2021. Precipitation of low-temperature disordered dolomite induced by extracellular polymeric substances of methanogenic Archaea *Methanosarcina barkeri*: Implications for sedimentary dolomite formation. Am Mineral, 106: 69–81
Zhao W, Walker S L, Huang Q, Cai P. 2014. Adhesion of bacterial pathogens to soil colloidal particles: Influences of cell type, natural organic matter, and solution chemistry. Water Res, 53: 35–46
Zheng W, Liu D, Yang S, Fan Q, Papineau D, Wang H, Qiu X, Chang B, She Z. 2021. Transformation of protodolomite to dolomite proceeds under dry-heating conditions. Earth Planet Sci Lett, 576: 117249

(Editorial handling: Rucheng WANG)